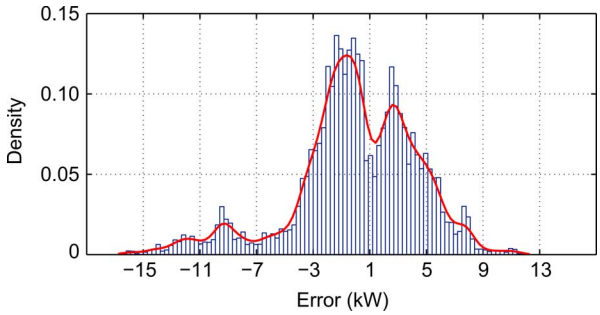

Fig. 4. Probability density of typical ANN error.

[14] that the consistency of the WLS state estimation relies on the assumption that measurements are normally distributed. In this work, the ANN error is processed using the GMM algorithm.

A GMM is the weighted finite sum of several Gaussian components. A multivariate GMM is characterized by a set of weights, mean vectors, and covariance matrices of the mixture components and mathematically can be expressed as

$$f(e|\gamma) = \sum_{i=1}^{M_c} w_i f\left(e|\mu_i, \sigma_i^2\right) \tag{7}$$

where M_c is the number of mixture components and w_i is the weight of the ith mixture component, subject to $w_i > 0$ and $\sum_{i=1}^{M_c} w_i = 1$. γ is chosen from the set of parameters $\Gamma = \{\gamma : \gamma = \{w_i, \mu_i, \sigma_i^2\}_{i=1}^{M_c}\}$, each member of which defines a Gaussian mixture. The density function of each mixture component $f(e|\mu_i, \sigma_i^2)$ is a normal distribution.

Details on the GMM formulation for load modeling in distribution systems can be found in [22].

In the proposed methodology, the error in each power injection estimate is modeled through a set of M_c mixture components. Then, each error is associated with a specific mixture component and the resulting variance is saved along with the corresponding error timestamp.

1) Error Association: An error is associated with the jth Gaussian component in the mixture through data association using the relative marginal density given by

$$f(j|e_i, \gamma) = \frac{w_j f(e_i|\mu_j, \sigma_j^2)}{\sum_{k=1}^{M_c} w_k f(e_i|\mu_k, \sigma_k^2)} = \frac{w_j \mathcal{N}\left(\mu_j, \sigma_j^2\right)(e)}{\sum_{k=1}^{M_c} w_k \mathcal{N}\left(\mu_k, \sigma_k^2\right)(e)}. \tag{8}$$

Using (8), the relative marginal density of the error at a specific time step with respect to each component is computed. The component with the maximum density is identified as representative of the error. If several components have comparable marginal densities, they can be merged together using the mixture reduction technique described in [13].

The error modeling concept is demonstrated in Fig. 5.

C. State Estimation Application

In the context of state estimation, the previously described ANN and error models are used to create the required power injection pseudo measurements. The execution of state estimation involves the following steps:

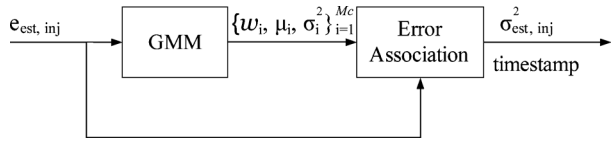

Fig. 5. Error modeling.

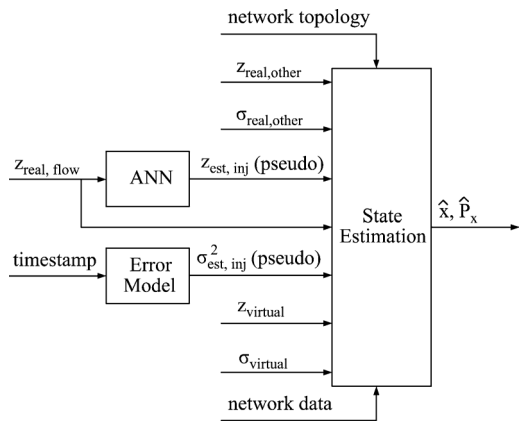

Fig. 6. State estimation application.

Step 1) At time t, use the real active and reactive power flow measurements as input to the ANNs.

Step 2) Obtain the active and reactive power injections at time t from the output of the ANNs and store them as pseudo measurements.

Step 3) Compare the output of ANN with the load values obtained from the load profiles and compute the error in pseudo measurements at time t.

Step 4) Associate the error computed in Step 3 with a GMM component in the error model and obtain the variance of active and reactive power injection pseudo measurements corresponding to this error.

Step 5) Use real and pseudo measurements along with their variances to construct the $\boldsymbol{R}_z$ matrix in (1) for state estimation.

Step 6) Repeat Steps 1 to 6 for other time steps.

Overall, the inputs to the state estimation function are real measurements (voltage magnitudes, active and reactive power flows, and active and reactive power injections), pseudo measurements (active and reactive power injections), virtual measurements (zero injection buses), and the network topology and parameters. All measurements are used with their corresponding standard deviations.

The state estimation execution concept is shown in Fig. 6.

V. Simulation Study

The performance of the proposed methodology was tested on a part of the U.K. Generic Distribution System (UKGDS) model. The 11-kV system considered comprises 95 buses, 94 lines, 54 loads and two DGs, as shown in Fig. 7. The system parameters and load information for the UKGDS were obtained from [23]. The buses were renumbered for convenience.

The UKGDS assumes four classes of consumers: Domestic-Unrestricted (D/U), Domestic-Economy (D/E), Industrial (I), and Commercial (C). Half hourly normalized active power load

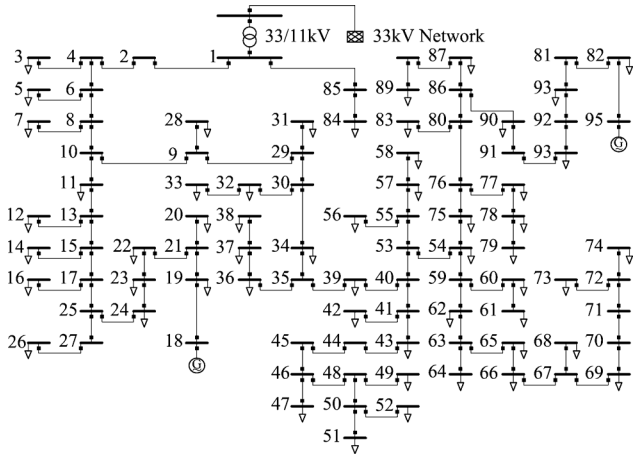

Fig. 7. Test network.

TABLE I
SUMMARY OF SCENARIOS

Scenario	ANN Input	Real Measurements
1	P_{1-2}, Q_{1-2}	V_1 $P_{1-2}, Q_{1-2}, P_{1-85}, Q_{1-85}$ $P_{18}, Q_{18}, P_{84}, Q_{84}, P_{95}, Q_{95}$
2	P_{1-2}, Q_{1-2} P_{15-17}, Q_{15-17} P_{34-35}, Q_{34-35}	V_1 $P_{1-2}, Q_{1-2}, P_{1-85}, Q_{1-85}$ $P_{15-17}, Q_{15-17}, P_{34-35}, Q_{34-35}$ $P_{18}, Q_{18}, P_{84}, Q_{84}, P_{95}, Q_{95}$
3	P_{1-2}, Q_{1-2} P_{15-17}, Q_{15-17} P_{34-35}, Q_{34-35}	$V_1, V_{19}, V_{20}, V_{21}$ $P_{1-2}, Q_{1-2}, P_{1-85}, Q_{1-85}$ $P_{15-17}, Q_{15-17}, P_{34-35}, Q_{34-35}$ $P_{18}, Q_{18}, P_{84}, Q_{84}, P_{95}, Q_{95}$

profiles over one year along with their annual maximum demand are provided for each consumer class. The methodology followed to obtain the load profiles from the mix of consumer classes at each bus is given in [23].

The three scenarios examined are presented in Table I. Voltage magnitudes and voltages angles are selected as the state variables in state estimation. Bus 1 is considered to be the reference bus with voltage angle equal to zero.

Two ANN variations for pseudo measurement modeling are considered. The first variation is based on the assumption that a single set of real power flow measurements is available at the substation (P_{1-2}, Q_{1-2}). The second variation uses two additional sets of power flow measurements (P_{15-17}, Q_{15-17} and P_{34-35}, Q_{34-35}), in accordance with the optimal measurement placement algorithm presented in [24].

Real measurements are assumed to be mainly available at the substation and the DG locations. Thus, the voltage magnitude at bus 1 (V_1), the active and reactive power flows in lines 1–2 and 1–85 (P_{1-2}, Q_{1-2} and P_{1-85}, Q_{1-85}), the active and reactive power injections at bus 18 and bus 95 (P_{18}, Q_{18} and P_{95}, Q_{95}) and, for completion, the active and reactive power injections at bus 84 (P_{84}, Q_{84}) were considered as real measurements in Scenario 1. The active and reactive power flows in lines 15–17 and 34–35 (P_{15-17}, Q_{15-17} and P_{34-35}, Q_{34-35}) were used as additional real measurements in Scenario 2. Additional voltage measurements at buses 19, 20, and 21 (V_{19}, V_{20}, and V_{21}) were considered in Scenario 3 in line with [24].

Real measurements were modeled by adding small Gaussian uncertainty to the values obtained from load flow. The values obtained from load flow were used as mean values and 3% error around the mean was added. The load flow values with Gaussian uncertainty were used as input to both the ANN and to the state estimation function, as shown in Fig. 6.

Pseudo measurements were modeled following the methodology presented in Section IV. The number of mixture components used in the majority of loads was two.

Virtual measurements with very low error (10^{-8}) were used to model zero injection buses.

The ANN training, the error modeling, and the state estimation execution covered a whole year with half-hour steps (17 520 time steps). However, for clarity, results are presented after being sampled every 100 h (88 samples).

VI. Results and Discussion

The estimated values of the voltage magnitude and angle estimates for bus 6 (close to the substation) and bus 74 (remote from the substation) for Scenario 2 along with their true values and their $\pm 3\sigma$ confidence bounds for their estimates are shown in Figs. 8–11. It is noted that all estimates are within the confidence bounds with voltage angle estimates following the shape of the true value of the voltage angle more consistently.

The same values for bus 74 for Scenario 3 are shown in Figs. 12 and 13. It is evident that the additional voltage measurements have increased the matching between true and estimated voltage values and have made the confidence bounds narrower. In addition, it is observed that the additional voltage measurements have very small influence in the voltage angle estimates.

In terms of statistical evaluation, the average relative error (normalized with respect to the true value) was used. The average relative voltage magnitude and voltage angle errors for a specific bus (excluding the reference bus) are computed as follows:

$$e_V(\%) = \frac{100}{N} \sum_i \left| \frac{\hat{V}^i - V_t^i}{V_t^i} \right| \tag{9}$$

$$e_\delta(\%) = \frac{100}{N} \sum_i \left| \frac{\hat{\delta}^i - \delta_t^i}{\delta_t^i} \right| \tag{10}$$

where $\hat{V}^i$ is the voltage magnitude estimate, V_t^i is the true voltage magnitude, $\hat{\delta}^i$ is the voltage angle estimate, δ_t^i is the true voltage angle, i is the sampling step, and N is the number of sampling steps.

Figs. 14–17 show the relative voltage magnitude and voltage angle errors for bus 74 for Scenario 1 and Scenario 2. It can be seen that in Scenario 2, where the ANNs have three inputs, the accuracy of the state estimator is significantly improved in comparison with Scenario 1, where the ANNs have a single input. From the results, it can be concluded that increasing the number of input to the ANNs and/or increasing the number of voltage measurements improves the accuracy of state estimation, as expected.

In the scenarios presented, 54 sets of active and reactive power injection pseudo measurements were modeled with ANNs using one set (Scenario 1) or three sets (Scenario 2

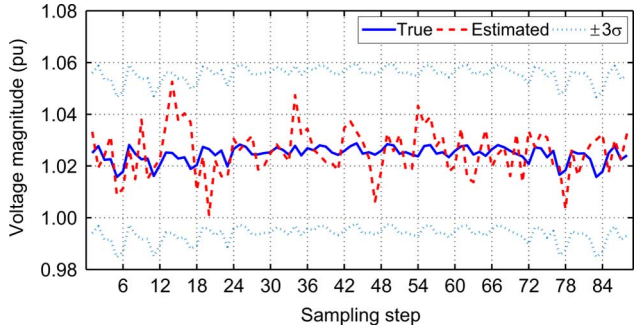

Fig. 8. Scenario 2—Bus 6 voltage magnitude.

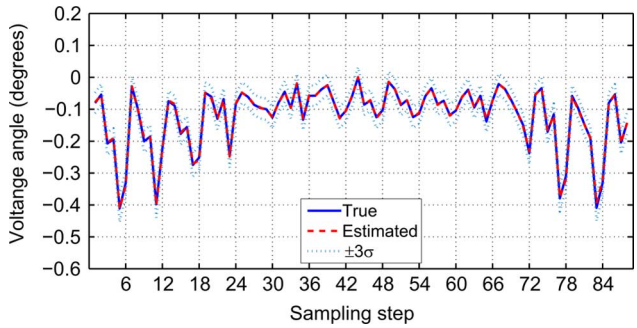

Fig. 9. Scenario 2—Bus 6 voltage angle.

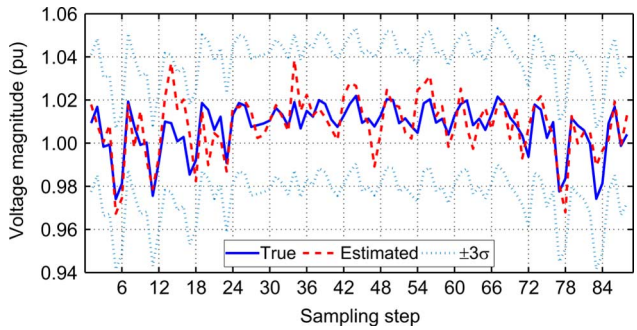

Fig. 10. Scenario 2—Bus 74 voltage magnitude.

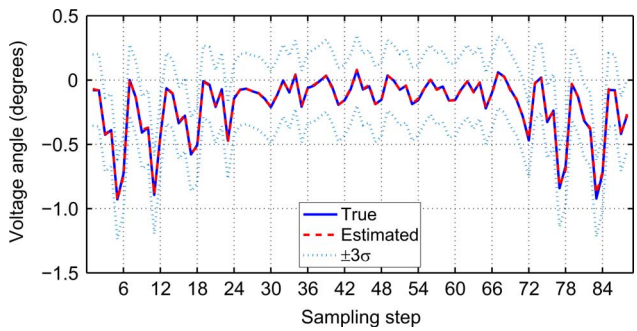

Fig. 11. Scenario 2—Bus 74 voltage angle.

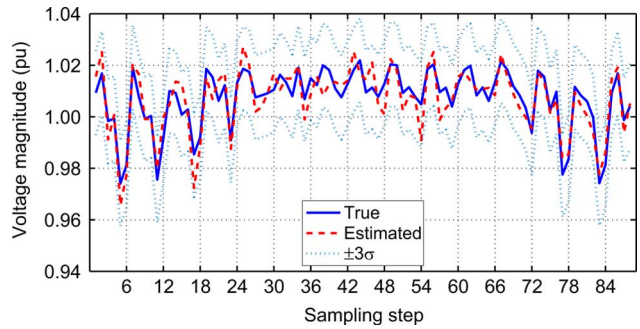

Fig. 12. Scenario 3—Bus 74 voltage magnitude.

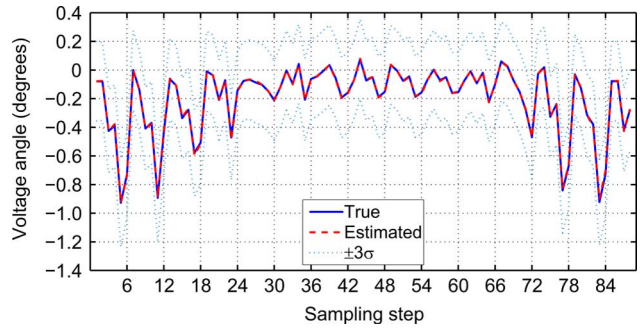

Fig. 13. Scenario 3—Bus 74 voltage angle.

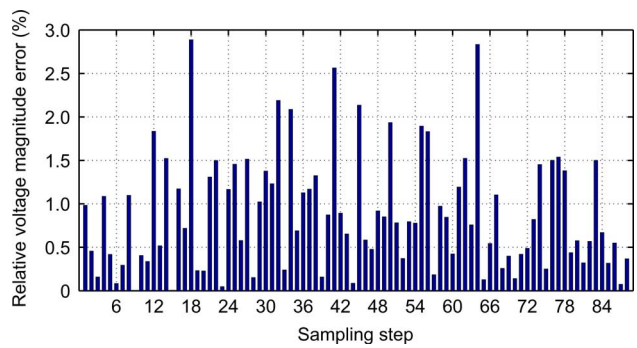

Fig. 14. Scenario 1—Bus 74 relative voltage magnitude error.

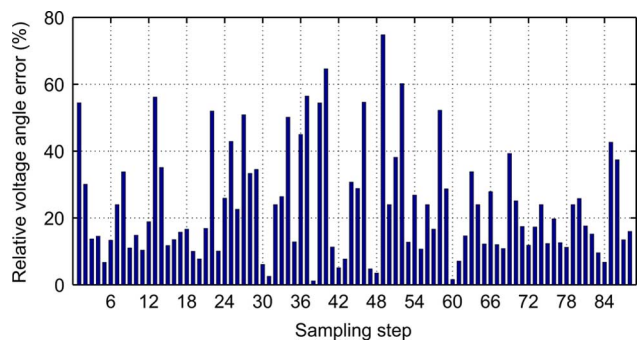

Fig. 15. Scenario 1—Bus 74 relative voltage angle error.

and 3) of real active and reactive power flow measurements. In effect, 54 sets of pseudo measurements were generated by monitoring 1% of the lines in Scenario 1 and 3% of the lines in Scenario 2 and 3 (the branch with buses 84 and 85 was ignored).

Table II presents the average relative voltage magnitude and voltage angle errors for bus 6 and bus 74 for all three scenarios and for both the ANN-based approach and using load profiles with 20% uncertainty as pseudo measurements. It is observed that although the average relative voltage magnitude error is similar (estimation of voltage magnitudes is directly affected by the available real voltage magnitude measurement in both cases), the proposed approach generates voltage angle estimates

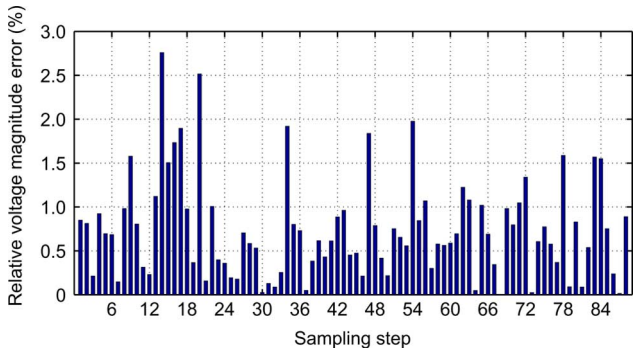

Fig. 16. Scenario 2—Bus 74 relative voltage magnitude error.

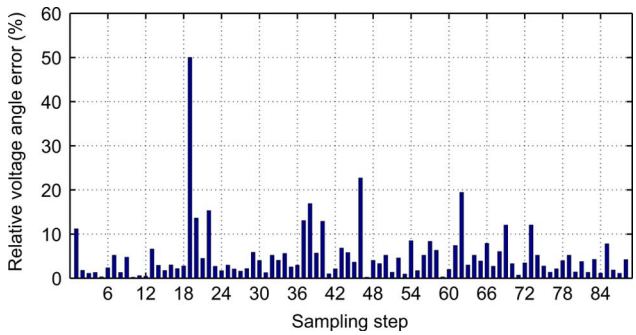

Fig. 17. Scenario 2—Bus 74 relative voltage angle error.

TABLE II
AVERAGE RELATIVE ERRORS

Scenario	State variable	Bus 6 (%)		Bus 74 (%)	
		ANN	Profile†	ANN	Profile†
1	Voltage magnitude	0.840	0.843	0.883	0.885
	Voltage angle	22.854	56.179	23.919	83.75
2	Voltage magnitude	0.711	0.799	0.741	0.847
	Voltage angle	4.404	40.310	5.180	64.08
3	Voltage magnitude	0.441	0.446	0.458	0.467
	Voltage angle	3.969	11.782	4.670	26.48

†20% error in load profile

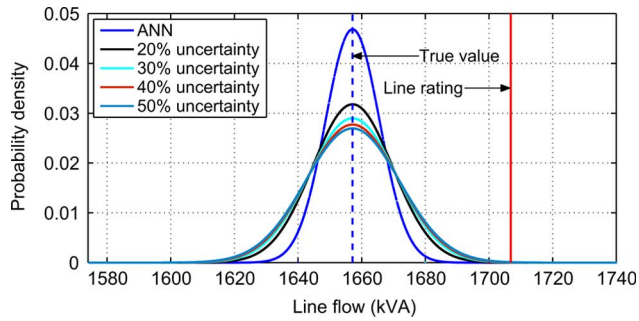

Fig. 18. Probability density of power flow estimate at line 2–4.

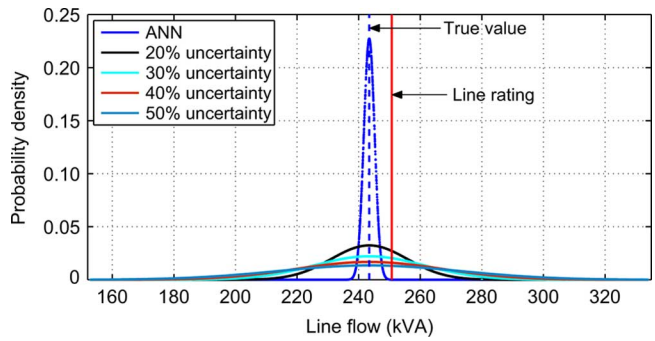

Fig. 19. Probability density of power flow estimate at line 10-11.

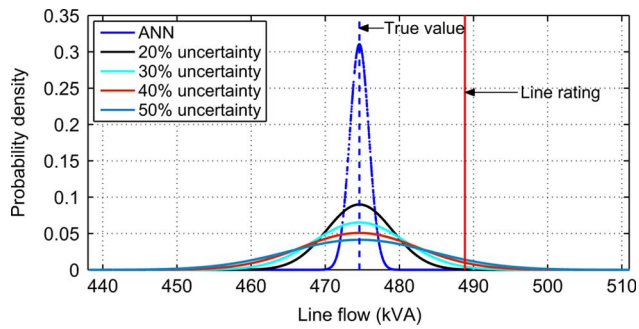

Fig. 20. Probability density of power flow estimate at line 72-74.

with significantly lower average relative error. Reducing the errors in the estimation of voltage angles is of particular importance as the accuracy of the computation of line power flows and currents is improved. As a result, equipment loading can be more effectively monitored.

In practice, voltage magnitude and angle estimates and estimation errors give limited insight to the distribution network operators (DNOs). DNOs are more interested in knowing the impact of estimates and estimation errors on the likelihood of a line being overloaded or a bus voltage magnitude being out of the statutory limits and their concern is whether this likelihood is captured by the state estimation function. As line power flows are functions of voltage magnitudes and voltage angle differences, any significant error in the voltage angle estimates will lead to poor line loading estimates. This is particularly important when lines operate close to their thermal limits.

In this context, the performance of the ANN-based approach is further evaluated through the accuracy of power flow estimates while lines are operating close to their thermal limits. To simulate this scenario, a snapshot of measurements on a typical winter day, when loads are high, is selected. The line power flows were estimated using the ANN-based pseudo measurement modeling approach. The true value of the line power flow was considered to be the mean of the estimate and its variance was computed using (6). To demonstrate the concept, it was assumed that the mean of the estimated power flows was around 97% of the line rating. Using the mean and variance, the probability densities of the estimated line power flows in all lines for Scenario 1 were computed.

The probability densities of power flow estimates in selected lines using the ANN-based approach are shown in Figs. 18–20. For comparison purposes, the probability densities of the estimated line power flows, computed using 20%, 30%, 40%, and 50% uncertainty in load pseudo measurements derived from average load profiles, are shown in the same figures. It is clear that the variation around the mean increases as the uncertainty in the load pseudo measurements increases. On the other hand, the variation is minimum in the case of the ANN-based approach.